DOI 10.4430/bgo00401

Seabed and shallow morphological setting of the western Sicilian Channel

V. Volpi, D. Civile, E. Lodolo, R. Romeo, D. Accettella, F. Accaino and G.M. Ferrante

Istituto Nazionale di Oceanografia e di Geofisica Sperimentale - OGS, Trieste, Italy

(Received: 28 March 2022; accepted: 14 July 2022; published online: 8 September 2022)

ABSTRACT The analysis of swath bathymetric data and high-resolution seismic profiles (CHIRP), combined with information from the literature, allowed the creation of an updated map of the topography of the seabed in the western part of the Sicilian Channel. This area includes the entire Adventure Plateau, the Pantelleria Graben, and the Capo Granitola-Sciacca offshore sector between the Sicilian coast, the Graham and the Terrible banks. Positive and negative bedforms (sedimentary banks, volcanoes and mud volcanoes, pockmarks) and some erosional features were recognised and analysed in the study area. The Capo Granitola-Sciacca offshore sector is a continental shelf characterised by the presence of various sand bodies that are locally cemented and interpreted as sand ridges, dunes and remnants of dune strands or barrier lagoon systems eroded by the action of bottom currents. These bodies were probably deposited during the post-LGM sea level rise, occurred from ca. 18 kyr B.P. and 6 kyr B.P. (transgressive deposits) and during the glacial phase (lowstand deposits) occurred about 20 kyr B.P., when sea level was ca. 120-130 m lower than today. In this area there are also several volcanic edifices, mud volcanoes and numerous pockmarks due to the presence of gas. The distribution of these bodies is controlled by the faults associated with the NNE-oriented active lithospheric structure called Capo Granitola-Sciacca Fault Zone, which crosses the entire western part of the Sicilian Channel. The northern margin of the rift-related Pantelleria Graben is punctuated by NW-oriented pockmarks, probably controlled by the faults bounding tectonic depression, where several scars and a broad landslide have been this also mapped. In addition, canyons were noted along the southern margin of the Adventure Plateau.

Key words: Sicilian Channel, seafloor morphology, western Mediterranean, multibeam swath bathymetry, high-resolution seismic profiles.

1. Introduction

The Sicilian Channel (SC) is still one of the least studied areas of the Mediterranean, both morphologically and structurally (Fig. 1). Compared to other Italian seas, such as the Tyrrhenian and Ionian seas, for which high-resolution bathymetric maps have long existed, less than 30% of its seabed has been mapped with modern high-resolution multibeam echo sounder technologies. However, this knowledge gap has narrowed in recent years, during which various geophysical and geological survey campaigns have been carried out in several sectors of the SC and particularly in its western part. These recent studies have mainly analysed: i) large-scale tectonic elements, seismostratigraphy and geophysical features (Finetti and Del Ben, 2005; Civile *et al*., 2010, 2014, 2016, 2018, 2021; Lodolo *et al*., 2012; Cavallaro *et al*., 2017; Fedorik *et al*.,

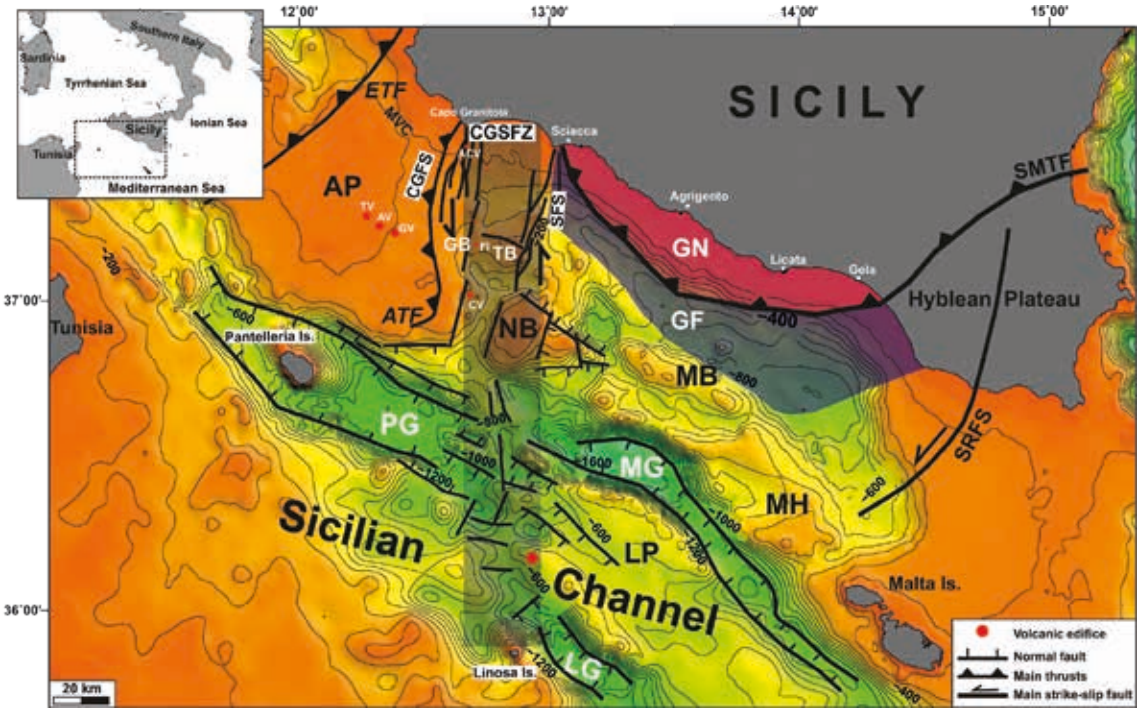

Fig. 1 - Structural map of SC (modified from Civile *et al.*, 2021). Abbreviations: ACV: Actea Volcano; AP: Adventure Plateau; ATF: Adventure Thrust Front; AV: Anfitrite Volcano; CGSFZ: Capo Granitola-Sciacca Fault Zone; CGFS: Capo Granitola Fault System; CV: Cimotoe Volcano; ETF: Egadi Thrust Front; FI: Ferdinandea Island; GB: Graham Bank; GF: Gela foredeep; GN: Gela Nappe; GV: Galatea Volcano; LG: Linosa Graben; MB: Madrepora Bank; MG: Malta Graben; MH: Malta High; MVC: Mazara del Vallo Channel; PG: Pantelleria Graben; SMTF: Sicilian-Maghrebian Chain Frontal Thrust; SRFS: Scicli-Ragusa Fault System; SFS: Sciacca Fault System; TB: Terrible Bank; TV: Tetide Volcano. The box in the upper left corner shows the location of the SC in the central Mediterranean Sea.

2018; Ferranti *et al*., 2019; Palano *et al*., 2020); ii) presence and characterisation of volcanic manifestations (Bosman *et al*., 2008; Coltelli *et al*., 2016; Lodolo *et al*., 2017, 2019a, 2019b, 2021; Cavallaro and Coltelli, 2019; Romagnoli *et al*., 2020); iii) specific morphological elements such as submerged banks and transgressive markers (Civile *et al*., 2015; Spatola *et al*., 2018a; Lodolo *et al*., 2020, 2022). However, an overall view is still lacking, due to the absence of a complete high-resolution bathymetric base over the entire geographical extent of the SC.

The present work focused on the recognition of morphological features in the western sector of the SC (Figs. 1 and 2), including the Pantelleria Graben, the Capo Granitola-Sciacca offshore sector up to the Graham and Terrible banks, and the Adventure Plateau (AP), where coverage is higher in bathymetric multibeam echo sounder data and very high-resolution seismic profiles, and where other 'vintage' geophysical data acquired in the 1970s and 1980s (mainly high-resolution seismic profiles) are available. The identified bedforms have been tentatively associated with various geological processes related both to the active tectonic structures identified in the study area and to the Last Glacial Maximum (LGM, ca. 20 kyr B.P.) and post-LGM evolution. The results presented in this paper integrate the morpho-bathymetric elements already reported in the literature and provide a more comprehensive and updated map of this sector of the SC.

2. Geological setting

Geologically, the SC (Fig. 1) belongs to the northern continental margin of the African Plate, the so-called Pelagian Block (Burrollet *et al*., 1978). The central-northern part of the SC shows an articulated morpho-bathymetry consisting of a series of shallow banks, the largest being the AP, small- to medium-sized and shallow structural banks, and NW-striking tectonic depressions that reach a maximum water depth of 1700 m in the Malta Graben (e.g. Civile *et al*., 2021). The banks are composed of Meso-Cenozoic carbonate and siliciclastic successions generally covered by a thin Plio-Quaternary succession, while the thickness of the Plio-Pleistocene basin fill varies from 800 m to over 2200 m in the Linosa Graben (Civile *et al*., 2021). This morphological setting is the result of the interaction of the following independent geodynamic processes (e.g. Jongsma *et al*., 1985; Boccaletti *et al*., 1987; Reuther *et al*., 1993; Catalano *et al*., 1996, 2002, 2013; Corti *et al*., 2006; Ben-Avraham *et al*., 2006; Argnani, 2009; Civile *et al*., 2010, 2014, 2016): i) the formation of the Neogene-Quaternary offshore part of the Sicilian-Maghrebian Chain in the northern and north-western part of the SC; ii) the continental rifting process that, since the early Pliocene, has produced the SC Rift Zone with the three prominent tectonic grabens of Pantelleria, Linosa and Malta, controlled by NW-trending subvertical normal faults. The central part of the SC is also crossed by the NNE-oriented Capo Granitola-Sciacca Fault Zone [CGSFZ, after Civile *et al*. (2018)], interpreted as an active lithospheric strike-slip transfer zone that extends for at least 200 km from the Sicilian coast between Capo Granitola and the town of Sciacca to the island of Linosa (Argnani *et al*., 1986; Antonelli *et al*., 1988; Argnani, 1990; Ghisetti *et al*., 2009; Calò and Parisi, 2014; Civile *et al*., 2018, 2021; Fedorik *et al*., 2018; Ferranti *et al*., 2019; Palano *et al*., 2020). The northern part of the CGSFZ consists of two major fault systems dominated by transpressional tectonics, the Capo Granitola Fault System (CGFS) to the west and the Sciacca Fault System (SFS) to the east (Fig. 1), separated by a 28-38 km wide, relatively flat area affected by gentle Pliocene to Quaternary tectonic deformation (Civile *et al*., 2018, 2021; Ferranti *et al*., 2019). Along the southern prosecution of the CGSFZ, between Nameless Bank and Linosa Island, no major tectonic lineaments are evident and the fault zone is characterised by an alternation of basins (up to about 1000 m deep) and prominent structural highs as the Bannock seamount (Civile *et al*., 2021). This 15-25 km wide area separates the Pantelleria Graben to the west from the Linosa and Malta grabens to the east (Argnani *et al*., 1986; Argnani, 1990; Civile *et al*., 2014, 2021). The study area includes most of the AP, the Capo Granitola-Sciacca coastline up to the Graham-Terrible banks, and the entire Pantelleria Graben (Fig. 2). The AP is a continental shelf morphologically separated from Sicily by the relatively deep (about 120 m water depth) Mazara del Vallo Channel (Civile *et al*., 2014, 2015). Several shallow banks [Talbot, Ante-Talbot, Nereo, Tetide, Anfitrite, Galatea, and Pantelleria Vecchia, (Fig. 2)], some of which are less than 10 m below sea level, punctuate the AP (Colantoni *et al*., 1985; Civile *et al*., 2015, 2016). Tetide, Anfitrite and Galatea banks are volcanic in origin, while the other sedimentary banks are remnants of a highly tectonised substrate, eroded during repeated phases of subaerial exposure (Colantoni *et al*., 1985; Calanchi *et al*., 1989; Civile *et al*., 2015).

The nearshore Capo Granitola-Sciacca sector is characterised by the presence of three main banks: Nerita, Graham and Terrible banks (Fig. 2). The NNE-SSW elongated Nerita Bank, which shallows to about 50 m below sea level, is an elliptical structural high controlled by a flower structure associated with the SFS (Civile *et al*., 2018). It is composed of siliclastic deposits of late Miocene age. The Terrible Bank is a triangular structural high composed of a Meso-Cenozoic carbonate sequence covered by Late Miocene siliciclastic deposits (Civile *et al*., 2018). Its top exhibits a terraced morphology that is very smooth in the eastern sector but rugged in the

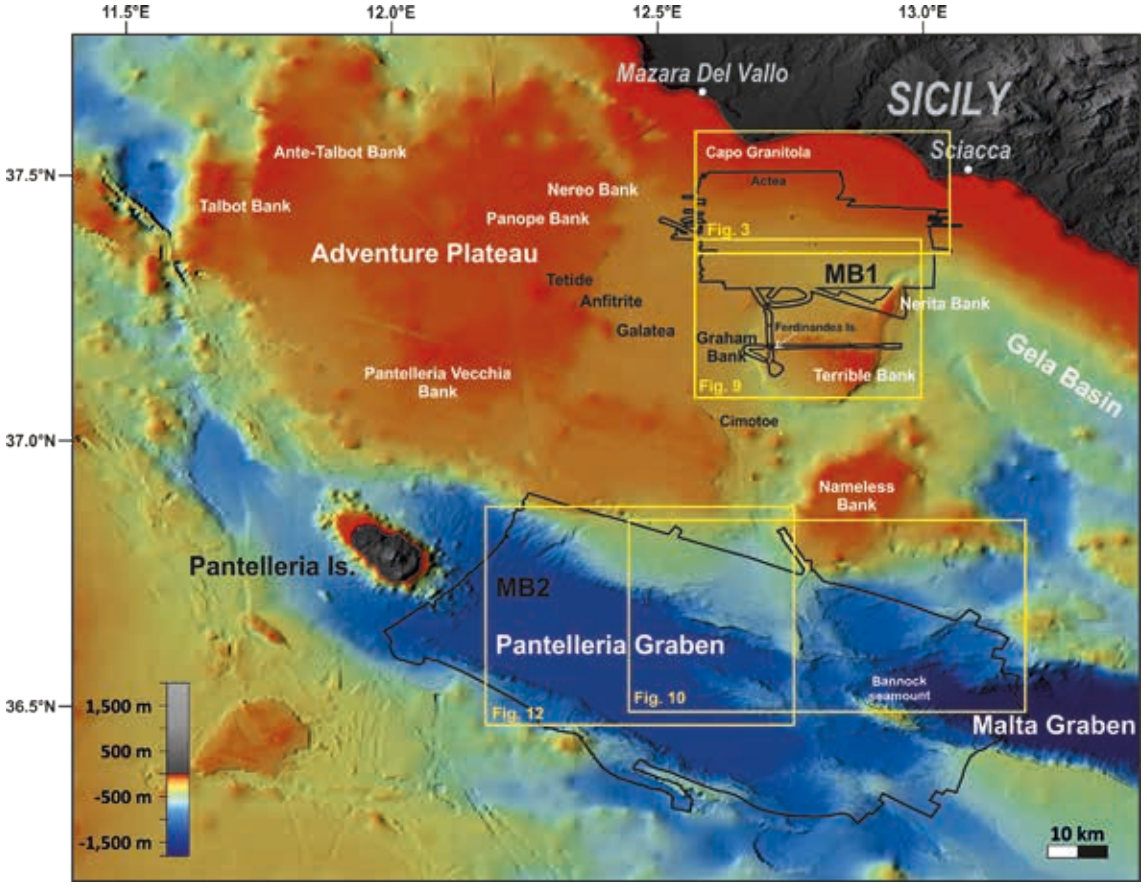

Fig. 2 – Morpho-bathymetric map of the SC, obtained from EMODnet (http://www.emodnet-bathymetry.eu/) Digital Terrain Model (1/16×1/16 arcmin), and multibeam data acquired by OGS (area delimited by black borders, MB1 and MB2). The position of the detailed morpho-bathymetric maps reported in Figs. 3, 9, 10, and 12 is also indicated.

western sector. Graham Bank consists of two shallow volcanic edifices, the smallest of which is the remnant of Ferdinandea Island (Fig. 2). These structures, along with eight other volcanic seamounts, are positioned along a N-S-striking belt located above the CGFS structures (Coltelli *et al*., 2016; Cavallaro and Coltelli, 2019). The Pantelleria Graben is about 125 km long and up to over 40 km wide in the Pantelleria Island area (Fig. 2), with a maximum water depth of 1350 m (Civile *et al*., 2010, 2021). Its eastern part has a rectangular shape with linear margins controlled by N115°-120° trending normal faults. The NE margin of the Pantelleria Graben consists of a steep escarpment up to 700 m high, while the SW margin has a gently dipping slope along its NW part, bordering a flat plateau area. Widespread magmatism is documented within the Pantelleria Graben and the largest magmatic body is represented by the partially outcropping volcanic complex of Pantelleria Island.

3. Data and methods

The bathymetric multibeam echo sounder data (Fig. 2) and high-resolution sub-bottom CHIRP seismic profiles analysed in this paper have been acquired by the R/V OGS Explora during two

surveys conducted in 2017 and 2018 as part of the 'FASTMIT' research project (MB1 area in Fig. 2), coordinated by the Istituto Nazionale di Oceanografia e di Geofisica Sperimentale (OGS) and funded by the Italian Ministry of University and Research (MIUR). These data incorporate data collected between 2009 and 2014 during scientific campaigns collected by OGS as strategic projects (MB2 area in Fig. 2). The high-resolution swath bathymetry was acquired using two keel-mounted Reson multibeam echo sounders (Reson Seabat 8111 for < 400 m water depth and Reson Seabat 8150 for full ocean depth). To achieve optimal data coverage, each swath overlapped neighbouring swaths by about 20%. Navigation data was collected using three integrated D-GPS systems. The acquired data, recorded using PDS2000® acquisition software, were fully corrected for vessel motion, navigation, sound speed and tides. Sound speed profiles were collected using a sound speed probe to correct for variations in sound speed in the water column. The data were processed (removal of residual peaks) and filtered, resulting in a Digital Terrain Model covering an area of 4455 km^2, with a grid cell size of 5×5 m^2 for the shallow areas and 25×25 m^2 for the deep areas. The visualisation of the data and the morphometric analysis of the bedforms (i.e. slope, elevation, areal extent) was done using Global Mapper® software. The freely available EMODnet digital terrain model (resolution 1/16×1/16 arcmin) was used (http://www.emodnet-bathymetry.eu/) to fill in the gaps not covered by the high-resolution bathymetric data.

The high-resolution CHIRP seismic profiles were acquired along the multibeam tracks using a hull-mounted Benthos Teledyne® CHIRP III DSP-665 for the FASTMIT area and CHIRP II for the 2009-2014 surveys (Fig. 2). The characteristic sweeps range from 2 to 7 kHz (vertical resolution is of the order of metres). The data were acquired with SwanPro® software and processed with Paradigm® software and Seismic Unix® using absorption compensation, migration and Hilbert transform.

In the CHIRP profiles, a generally highly visible reflector with high amplitude and continuity was interpreted as the LGM unconformity, as previously proposed by several authors (Civile *et al*., 2015, 2018; Ferranti *et al*., 2019; Lodolo *et al*., 2019a, 2020, 2022). This surface marks the exposed landscape and thus represents the shelf-scale erosional unconformity related to the LGM. It is a composite surface formed first by subaerial erosion associated with global glacier-induced sea-level retreat, which peaked ca. 20 kyr B.P. when sea level was about 120-130 m below present level, and then by wave action during post-LGM marine transgression.

4. Results

4.1. Positive features

4.1.1. Sedimentary banks of the Adventure Plateau

The geophysical and geological surveys carried out in the late 1970s and 1980s indicated the presence of various bathymetric elevations within the AP (Borsetti *et al*., 1974; Colantoni, 1975; Colantoni *et al*., 1985). Based on sample analysis and seismic data, the Talbot, Ante-Talbot, Nereo, and Pantelleria Vecchia elevations have been interpreted as sedimentary banks (Fig. 2) consisting of pre-Pliocene deformed and eroded carbonates and sandstones with a thin or absent Quaternary cover (Borsetti *et al*., 1974; Colantoni, 1975; Colantoni *et al*., 1985; Civile *et al*., 2015, 2016). High-resolution bathymetric data and CHIRP profiles made it possible to define the morphological and structural characteristics of these banks, as described in Civile *et al*. (2015, 2016).

4.1.2. Volcanic edifices

Several Quaternary submarine volcanic edifices have already been recognised in the NW sector of SC. In particular, the origin of the volcanoes located in the nearshore area between the Capo Granitola-Sciacca coast of Sicily (Lodolo *et al*., 2019a), in Graham Bank (Coltelli *et al*., 2016; Cavallaro and Coltelli, 2019) and Terrible Bank (Colantoni *et al*., 1975; Falzone *et al*., 2009; Coltelli *et al*., 2016; Civile *et al*., 2018; Cavallaro and Coltelli, 2019; Lodolo *et al*., 2019b) and along the eastern margin of the AP (e.g. Cimotoe Volcano in Fig. 2) (Calanchi *et al*., 1989; Civile *et al*., 2021) have been associated with magma ascent along the CGFS and SFS lithospheric faults (Civile *et al*., 2018). Three other volcanic edifices (Tetide, Anfitrite and Galatea) are located in the central part of the AP along a nearly 10 km long, N120°-oriented alignment (Calanchi *et al*., 1989; Civile *et al*., 2015, 2016). This alignment is parallel to the axis of the Pantelleria Graben and may indicate an origin related to the presence of NW-striking faults associated with the development of the SC Rift Zone (Civile *et al.*, 2014, 2015).

4.1.3. Sedimentary bodies

Type 1. A series of parallel and generally symmetrical ridges extending towards NW-SE are located 1-1.5 km west of the Actea Volcano, which is the edifice closest to the coast, in water depths ranging between 68 and 77 m (Fig. 3). It is possible to identify a northern field consisting of four main ridges close to each other, with a variable wavelength between 170 and 280 m, and a single southern body characterised by a different morphology with a horseshoe-shaped southern part (Fig. 3). The northern ridges, which are up to 2-3 m high, have a variable length between 600 m and over 1 km, a width between 80 and 250 m and slope values of the flanks of 1-5°. The south-western flanks of the ridges are generally more pronounced and inclined,

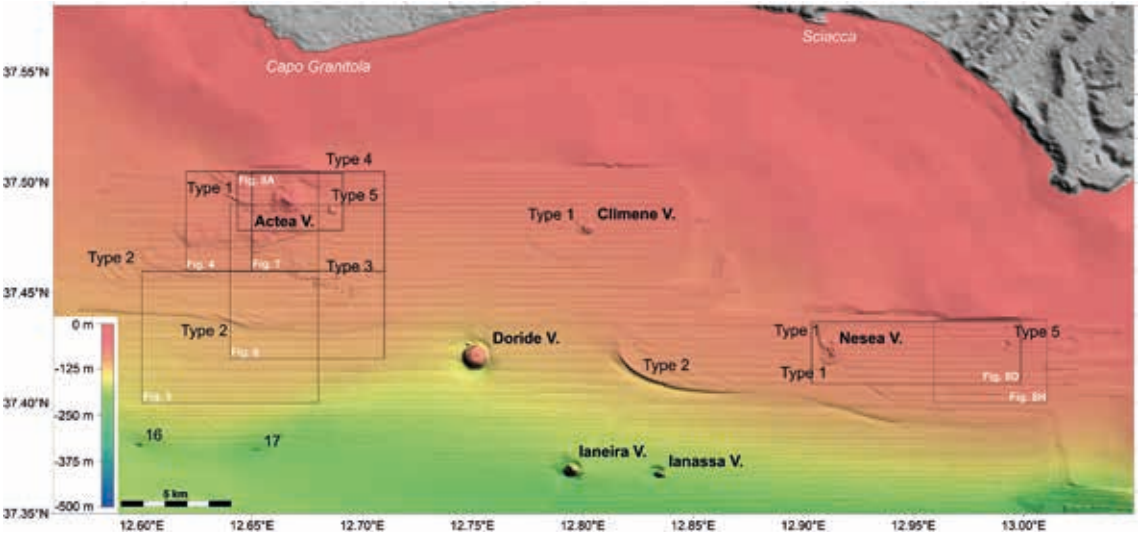

Fig. 3 - Morpho-bathymetric map of the Capo Granitola-Sciacca coastal sector, showing the locations of the positive (Types 1 to 5) and negative features described in the text. The position of the six volcanoes identified by Lodolo *et al*. (2019a) (Actea, Climene, Nesea, Doride, Ianeria and Ianassa) are also indicated. The black rectangles indicate the position of the detailed morpho-bathymetric maps shown in Figs. 4 to 8. The position of the morpho-bathymetric map is indicated in Fig. 2.

compared to the north-eastern ones. The southern single ridge is about 1800 m long and up to 400 m wide. The flanks have slope values of 4-5°, and the south-western flank is characterised by a steep step up to 8 m high. These ridges show opaque seismic facies with no internal reflectors covered by a very thin layer of recent sediments, and are located above the LGM subaerial unconformity, as seen from CHIRP profiles (Fig. 4): the presence of these bodies limits the penetration of the seismic signal, suggesting that they may be composed of coarse-grained and probably cemented sediment. Other modest reliefs with the same characteristics are located in the immediate vicinity of the Climene and Nesea volcanoes (Fig. 3).

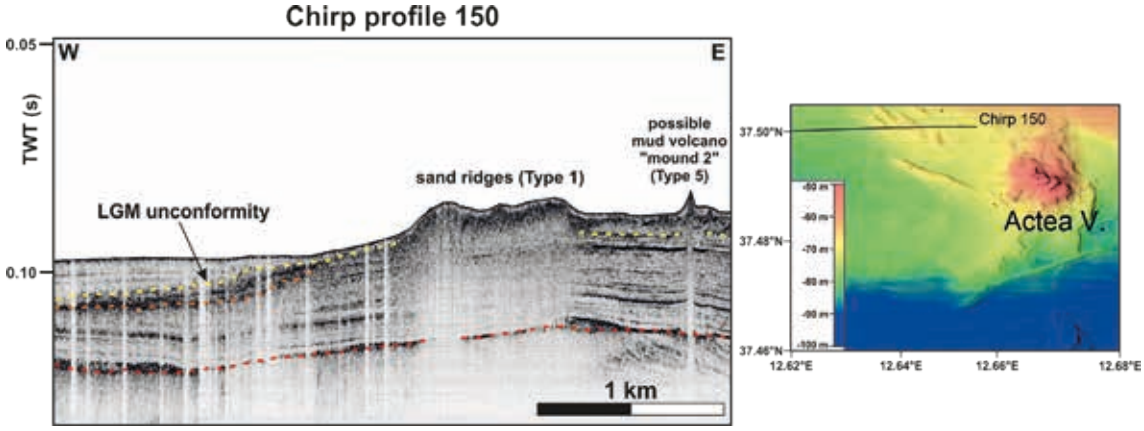

Fig. 4 - High resolution CHIRP profile 150, crossing the Type 1 features interpreted as sand ridges and located NW of the Actea Volcano. The reliefs are up to 8 m high and are characterised by opaque seismic facies with no internal reflections due to poor seismic signal penetration. A small positive feature (Type 5), interpreted as a possible mud volcano, is visible on the right side of the seismic profile. The position of the detailed morpho-bathymetric map is shown in Fig. 3.

Type 2. Two distinct fields, consisting of several thin arcuate ridges (60 to 300 m wide) and extending in a variable direction from NW-SE to about E-W, are located south and SE of the prominent lava flow of Actea Volcano, on the continental shelf, where water depths range from 92 to 115 m (Fig. 3). These bodies generally have a rather steep SW flank with inclination values of 2-3° and a very gently inclined NE side. The ridges of the northern field have a variable length between 500 and 1400 m and are bounded to the SW by up to 2-3 m high scarps. The southern field consists of contiguous bodies with a variable length between 600 and 3600 m and a prominent SW flank up to 6-7 m high (Fig. 3). In the high-resolution seismic profiles, these bodies are asymmetric with moderate relief, with a more inclined SW flank compared to the NE flank, and show no sedimentary cover lying on the LGM unconformity (Fig. 5). These bodies are characterised by semi-transparent seismic facies containing low-amplitude SW tilted reflectors interpreted as prograding foresets (clinoforms). Another field consisting of NW-trending thin arcuate asymmetric ridges, with a length between 600 and 1200 m, is located between Doride and Nesea volcanoes at water depths between 96 and 105 m (Fig. 3).

Type 3. About 2.5-3 km SE of the prominent lava flow of Actea Volcano, an area of 6.7 km^2 in water depths between 98 and 103 m, several strongly eroded mounds and pinnacles have been identified (Fig. 3). These can be isolated bodies or arranged in arcuate structures up to 1.4 km long and 200 m wide, characterised by a NW-oriented west side and a NE-oriented east side.

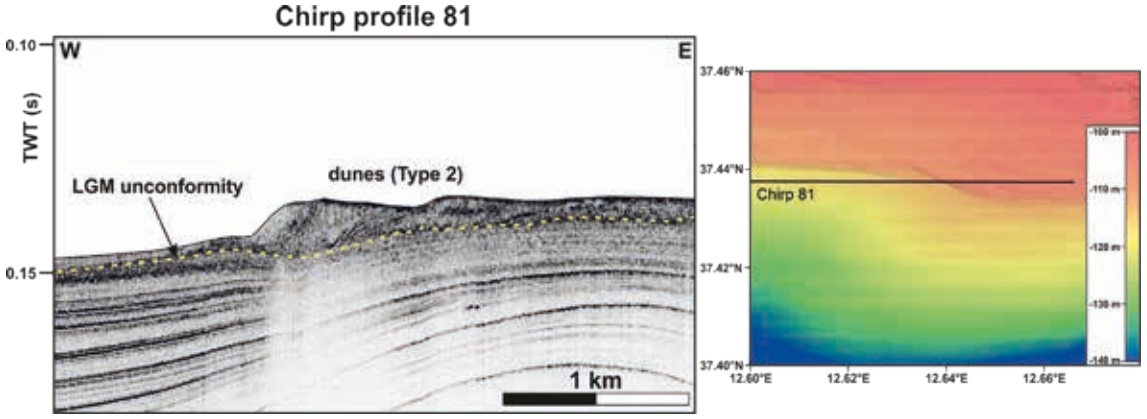

Fig. 5 - High-resolution CHIRP profile 81, crossing the positive Type 2 reliefs interpreted as dunes. They consist of a series of buried or outcropped asymmetrical bodies composed of SW dipping, prograding clinoforms resting on the LGM unconformity. These bodies do not allow good penetration of the seismic signal, suggesting a sandy nature. The position of the detailed morpho-bathymetric map is shown in Fig. 3.

The height of these reliefs ranges from 2 to 8 m, while the inclination of their flanks is 3-7°. The CHIRP profile (Fig. 6), which crosses these features, shows the presence of mounds and pinnacles separated by erosive incisions locally covered by a thin recent deposit. These bodies lie on the LGM unconformity, which truncates an underlying deformed sedimentary body associated with the Capo Granitola positive flower structure (Civile *et al.*, 2018).

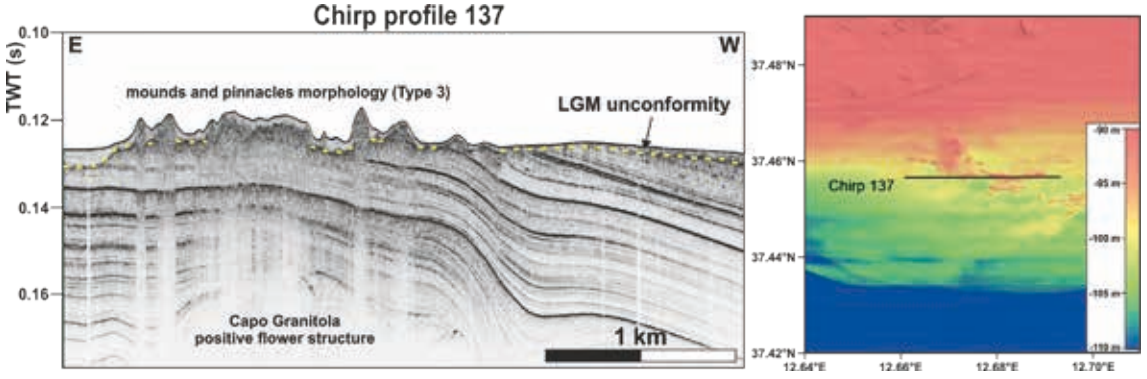

Fig. 6 - High-resolution CHIRP profile 137, crossing positive Type 3 features, SE of Actea Volcano. The position of the detailed morpho-bathymetric map is shown in Fig. 3. The morphology of the seabed consists of mounds and pinnacles separated by erosive incisions filled by a thin layer of recent sediments. These features lie on the LGM unconformity and are characterised by an opaque seismic facies. The pre-Neogene sequence is tectonically deformed by the positive flower structure of the Capo Granitola fault zone.

Type 4. A low, rounded mound extending E-W for 1.8 km and N-S for 1 km is located at a water depth ranging from 66 to 70 m, near Actea Volcano to the NE (Fig. 3). This mound, which becomes thinner towards the south, extends over 1.2 km^2 and is up to 6 m high (Fig. 7). It is bounded by a moat running NW along its western flank. The slope of the flanks is about 1°. The CHIRP profile in Fig.7 shows a semi-transparent seismic facies with parallel and discontinuous

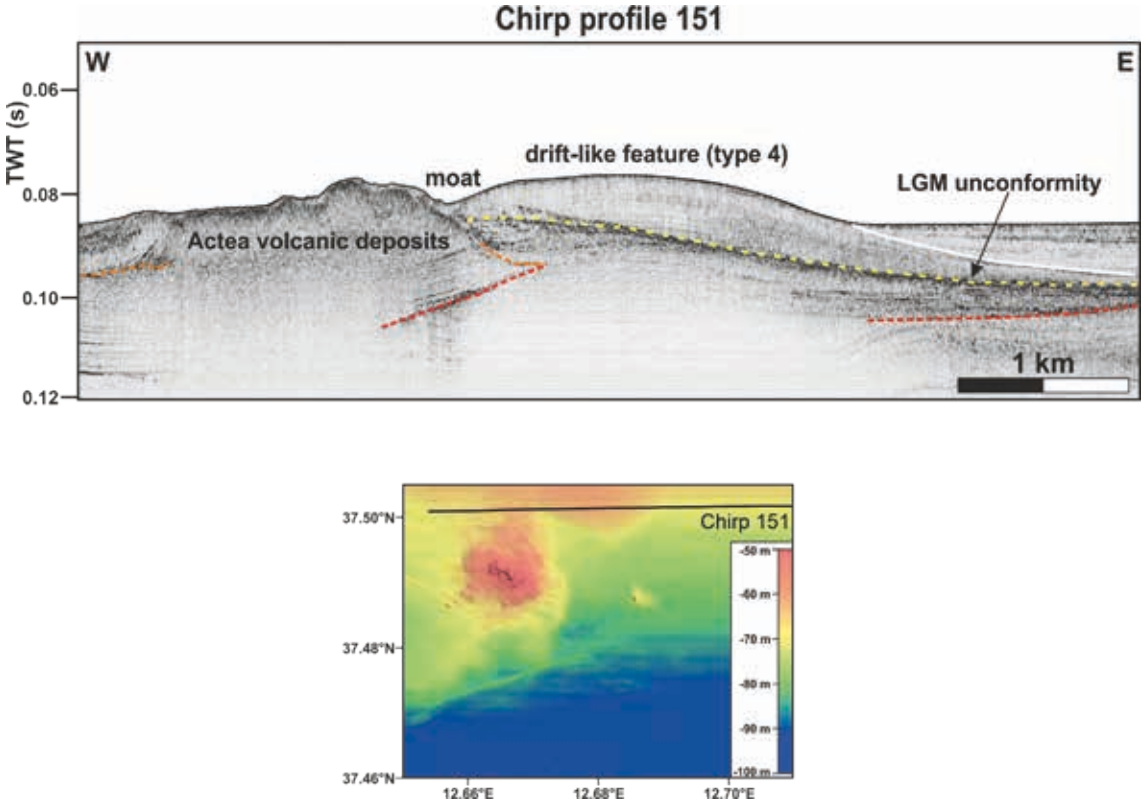

Fig. 7 - High-resolution CHIRP profile 151 crossing Type 4 feature located NE of the Actea Volcano. It is a rounded mound characterised by an asymmetric shape that is more inclined on the west side and smoother on the east side, similar to a sediment drift. The internal weak reflectors follow the shape of the mound and overlie the LGM unconformity to the west and overlie the same surface downwards on the east. This mound is overlain to the east by a younger unit consisting of horizontal reflectors. The location of the detailed morpho-bathymetric map is shown in Fig. 3.

low-amplitude reflectors following the shape of the mound. These reflectors overlap the LGM unconformity to the west, while to the east they follow it. This rounded mound is overlain by a younger unit with horizontal reflectors.

Type 5. Several modest elliptical and sub-circular reliefs, characterised by the absence of associated magnetic anomalies (see the 3D map of magnetic anomalies in Lodolo *et al*., 2019a), were observed near the volcanic edifices of Actea and Nesea (Fig. 3). They have an areal extent between 0.004 and 0.032 km^2 and a height between 1 and 4 m, except for the largest structure east of the Actea Volcano with an area of 0.155 km^2 and a height of 10 m. We have numbered them from west to east, starting with the mounds located near the Actea Volcano (Fig. 8A) and ending with the group of mounds east of the Nesea Volcano (Fig. 8D). Table 1 lists their main features. The largest mound 1 (Figs. 8A and 8B) is located 800 m east of the Actea Volcano, in a water depth ranging between 77 and 81 m. The surface of the mound has a rugged morphology. Small mound 2 (Figs. 8A and 8C) lies about 1.5 km NW of Actea Volcano in a water depth ranging from 69 to 70 m. This mound, characterised by a pointed summit in 66-m water depth, can be seen on the CHIRP profile in Fig. 4. It appears as an acoustically opaque small relief that does not allow signal penetration and creates a kind of vertical channel along which a pull-up effect of the reflectors occurs, possibly caused by the vertical migration of muddy sediments.

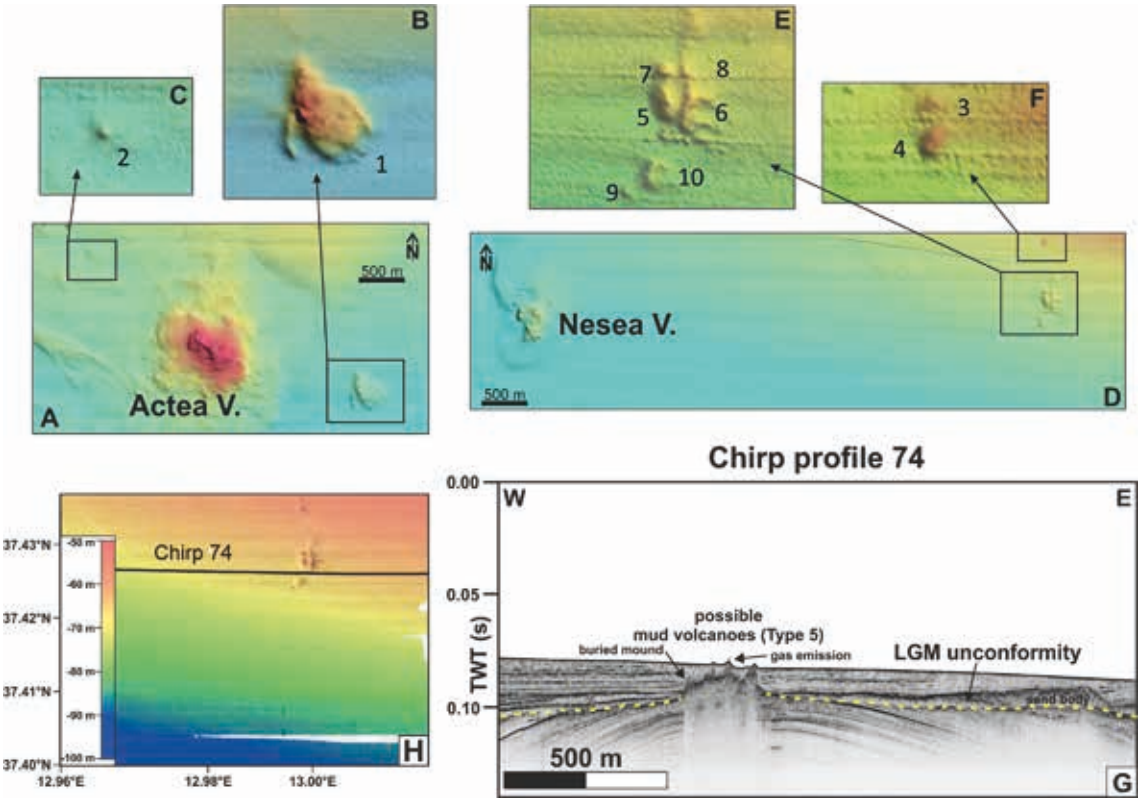

Fig. 8 - Type 5 features identified and interpreted as possible mud volcanoes in the Capo Granitola-Sciacca coast near the Actea Volcano (A) and east of the Nesea Volcano (D); B) the large mound east of the Actea Volcano; C) the small mound NW of the Actea volcano; E) and F) modest reliefs arranged in three groups along a 2-km-long N-S-oriented belt, about 7 km east of the Nesea Volcano. The characteristic parameters of these mounds are listed in Table 1; G) CHIRP Profile 74, which crosses the southern part of the N-S oriented belt (H), evidences three small reliefs with an opaque seismic facies on the seabed and a buried mound. They lie on a probable buried sand body, creating a blanking effect. Gas emission from the top of the central outcropping mound is visible as well as a bending of the recent sediments. The mounds are located on a folded pre-LGM sequence and in particular along the hinge of an anticline. The location of the detailed morpho-bathymetric map (H) is shown in Fig. 3.

Modest reliefs organised in three clusters are aligned along a 2-km-long, N-S-oriented belt located about 7 km eastwards from the Nesea Volcano (Figs. 8D-8F), at a water depth ranging between 59 and 68 m. The water depths of the summit of the mounds vary between 61 and 59 m, whereas their height on the seafloor ranges between 1 and 4 m. The CHIRP profile in Fig. 8G crosses the southernmost cluster of mounds and evidence three small reliefs with an opaque seismic facies at the seafloor and a buried mound. They lie on a probably buried sand body that produces a blanking effect. Gas emission from the top of the central outcropping mound is visible, as well as a bending of the recent sediments. The mounds are located on a folded pre-LGM succession, and in particular along the hinge of an anticline that is typically a zone affected by considerable brittle deformation, which could be responsible for the rising of fluids. Along the NS-oriented belt have been identified several gas emissions in the water column and gas-related features in the subsurface as bright spots (Ferrante *et al.*, 2022).

Table 1 - Measured parameters of the Type 5 mounds.

N	Area (km^2)	Shape	Diameter (m)	Length (m)	Width (m)	Height (m)	Slope (°)
1	0.155	elliptical		550 (NNW-SSE)	450	10	12 max
2	0.004	elliptical		95 (NE-SW)		3.5	3 - 12
3	0.0075	elliptical		115 (N-S)	80	1	2 - 4
4	0.007	subcircular	60			3	1 - 3
5	0.016	elliptical		100 (NW-SE)	42	3	2 - 7
6	0.032			100 (NE-SW)	50	3	2 - 8
7	0.004	subcircular	70			4	12 (max)
8	0,0025	subcircular	70			2	12 (max)
9	0.0025	subcircular	70			3	18
10	0.016	subcircular	150			3	3 - 8

4.2. Negative features

4.2.1. Seafloor depressions

Analysis of the high-resolution multibeam echo sounder data obtained west of the Nerita Bank and on the northern flank of the Pantelleria Graben revealed the presence of two series of mainly sub-circular/elliptical seabed depressions (67 in total) with variable depths (from a few to more than 10 m) and areal extent varying from 0.01 to 0.04 km^2, sometimes up to 0.08 km^2 (Figs. 9 and 10). Table 2 summarises the parameters measured for each feature. The northern alignment, about NW-SE, has a NW extremity curving towards SW. It consists of 34 depressions located in water depths ranging between 170 m and 240 m (Figs. 9A to 9D). In addition, five isolated features deviate from the main alignment: two of them are located 2 km north of the northern end of the main alignment (Fig. 9B, numbers 16 and 17), and the other three are located 8 km NE from the SE end of the alignment (Fig. 9D, numbers 28-30).

A total of 24 sub-circular depressions have been identified along the north-eastern side of the Pantelleria Graben (Figs. 10AD to 10C, numbers 40-63). These depressions generally form NW-SE alignments parallel to the graben axis, which is controlled by normal faults with the same trend. Another NW-SE aligned group of 4 depressions (Figs. 10A and 10D, numbers 64-67) is visible along the NW margin of the Malta Graben. The seismic data show that all sub-seafloor structures are not covered by recent sedimentation and have continuous high-amplitude reflectors with concave-upward geometry. In the sub-seafloor, there are hyperbolic anomalous signal distortions most likely caused by physical disturbances in the sediments during the escape of gas generated further down (Fig. 11). However, CHIRP profiles acquired across the depressions show no evidence of gas leakage in the water column.

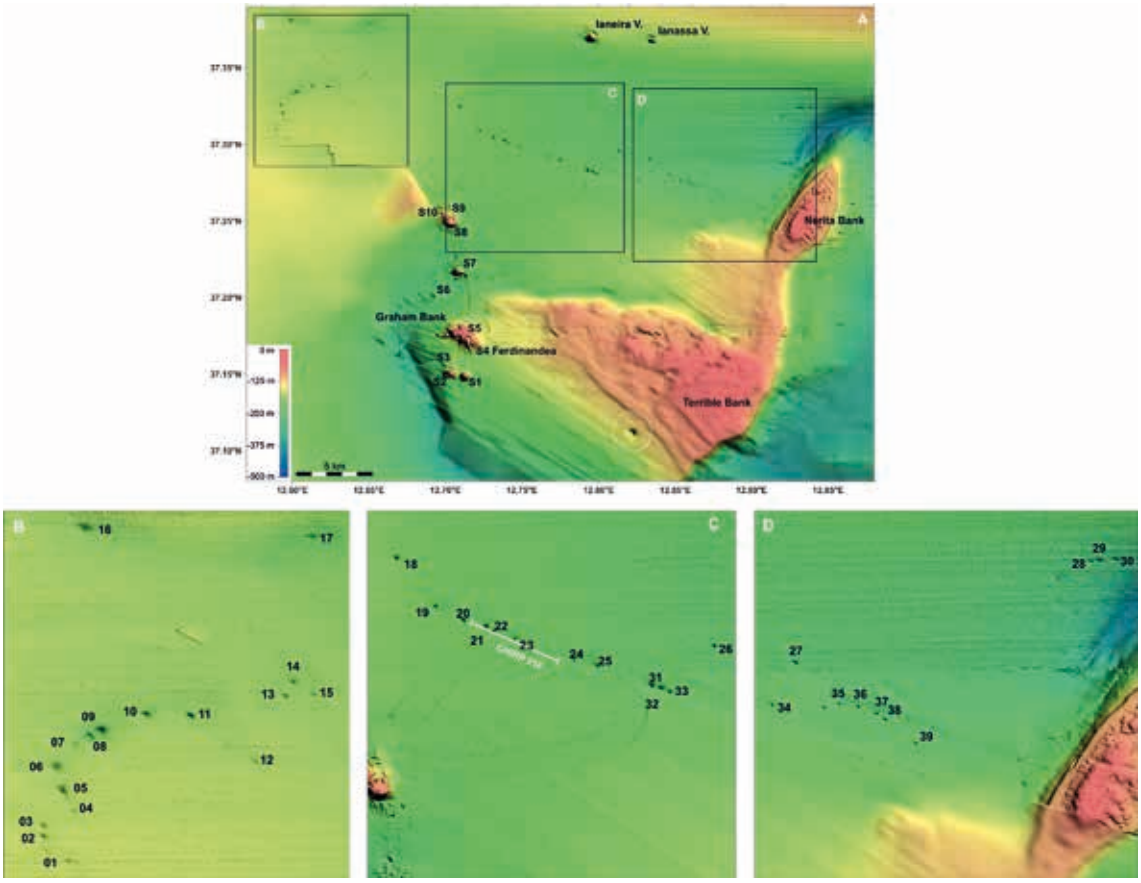

Fig. 9 - Negative features present in the northern part of the study area between Terrible Bank and the coast of Sicily (A). These negative features, interpreted as pockmarks, are sub-circular/elliptical depressions of the seabed. The seabed depressions form an approximately NW-SE aligned line whose NW end curves towards SW (A to D). It consists of 34 depressions in water depths ranging from 170 to 240 m. South of Terrible Bank is the largest pockmark identified in the area (white circle in Fig. 9A) (Coltelli *et al*., 2016). The position of the main morpho-bathymetric map (A) is shown in Fig. 2.

Table 2 - Parameters measured for the identified seafloor depressions on the AP and the northern flank of Pantelleria Graben.

Id	Lon [d.ddd°E]	Lat [d.ddd°N]	Plan view	Cross-section	Major axis [m]	Minor axis [m]	Surface base [km^2]	Top depth [m]	Depth [m]
1	12.59465310	37.30365964	sub-circular	V-shape	140	122	0.01279	-165	2
2	12.58879123	37.30952414	sub-circular	V-shape	222	201	0.03431	-168	5
3	12.58895928	37.31203285	sub-circular	V-shape	213	203	0.03376	-169	5
4	12.59588507	37.31527390	sub-circular	V-shape	47	46	0.001597	-171	1
5	12.59308937	37.32014650	elliptical (N-S)	V-shape	335	255	0.000805	-173	11
6	12.59163448	37.32542484	sub-circular	V-shape	310	290	0.0735	-177	13
7	12.59654258	37.33111202	elliptical (NE-SW)	V-shape	159	61	0.00987	-185	1
8	12.59981919	37.33276465	elliptical (NE-SW)	V-shape	172	123	0.01566	-201	5
9	12.60201537	37.33397173	elliptical (NE-SW)	V-shape	240	147	0.02582	-196	9

Table 2 - continued.

Id	Lon [d.ddd°E]	Lat [d.ddd°N]	Plan view	Cross-section	Major axis [m]	Minor axis [m]	Surface base [km²]	Top depth [m]	Depth [m]
10	12.61258535	37.33769122	sub-circular	V-shape	234	198	0.0374	-185	10
11	12.62286516	37.33740267	sub-circular	V-shape	233	206	0.03874	-185	13
12	12.63783117	37.32659095	sub-circular	V-shape	133	125	0.01305	-176	2
13	12.64494522	37.34198095	sub-circular	V-shape	187	166	0.02422	-184	5
14	12.64669928	37.34508893	sub-circular	V-shape	212	176	0.02969	-186	6
15	12.65135973	37.34223471	sub-circular	V-shape	123	119	0.01068	-185	2
16	12.59824696	37.38032394	elliptical (NW-SE)	V-shape	392	250	0.0762	-188	13
17	12.65099856	37.37843721	elliptical (E-W)	V-shape	333	200	0.053	-202	5
18	12.70905137	37.32433323	sub-circular	V-shape	225	222	0.0425	-200	16
19	12.72176984	37.30861860	sub-circular	V-shape	203	190	0.03007	-206	13
20	12.73088786	37.30405352	sub-circular	V-shape	232	209	0.03812	-211	16
21	12.73840367	37.30209764	sub-circular	V-shape	256	242	0.04677	-212	18
22	12.74096354	37.30062351	sub-circular	V-shape	182	161	0.02335	-212	10
23	12.74773119	37.29801288	sub-circular	V-shape	124	116	0.01053	-216	7
24	12.76691871	37.29080644	sub-circular	V-shape	110	108	0.00845	-222	5
25	12.77433421	37.28911671	sub-circular	V-shape	197	180	0.02615	-226	11
26	12.81296988	37.29563210	sub-circular	V-shape	136	129	0.01389	-241	11
27	12.83305921	37.29017986	sub-circular	V-shape	243	180	0.03295	-247	13
28	12.92993450	37.32297123	sub-circular	V-shape	108	80	0.00602	-283	3
29	12.93230164	37.32348128	elliptical (E-W)	V-shape	224	131	0.02375	-284	7
30	12.93753293	37.32366274	sub-circular	V-shape	146	113	0.01365	-292	6
31	12.79205186	37.28264449	sub-circular	V-shape	294	235	0.05310	-230	15
32	12.79516629	37.28181937	sub-circular	V-shape	233	183	0.03214	-230	12
33	12.79806833	37.28053961	sub-circular	V-shape	182	150	0.02104	-228	9
34	12.82510235	37.27623610	sub-circular	V-shape	168	147	0.02111	-231	5
35	12.84726209	37.27666837	sub-circular	V-shape	160	112	0.01433	-246	6
36	12.85331232	37.27568780	sub-circular	V-shape	157	120	0.01609	-249	7
37	12.85927031	37.27357871	sub-circular	V-shape	160	128	0.01721	-250	8
38	12.86212429	37.27155748	sub-circular	V-shape	155	132	0.01576	-248	7
39	12.87223967	37.26395313	sub-circular	V-shape	130	109	0.01124	-240	6
40	12.42790842	36.78566667	sub-circular	V-shape	106	80	0.00562	-545	4
41	12.43473581	36.78374365	sub-circular	V-shape	125	105	0.01129	-545	8
42	12.44008724	36.78253197	elliptical (WNW-ESE)	V-shape	107	74	0.0055	-545	5
43	12.44378607	36.78184327	elliptical (WNW-ESE)	V-shape	211	94	0.0152	-546	5
44	12.45111007	36.78016879	elliptical (E-W)	V-shape	229	141	0.02473	-544	15
45	12.48446306	36.76333453	elliptical (E-W)	V-shape	232	141	0.02473	-544	15
46	12.48909813	36.76096763	sub-circular	V-shape	185	147	0.01935	-551	14
47	12.49575641	36.75882567	elliptical	V-shape	179	127	0.01911	-554	8
48	12.48742183	36.74851550	sub-circular	V-shape	104	93	0.00759	-568	6
49	12.47112044	36.74207990	elliptical (E-W)	V-shape	202	103	0.01757	-614	10
50	12.53940767	36.75118866	elliptical (E-W)	V-shape	149	108	0.01397	-560	10
51	12.52897246	36.72770897	elliptical NE-SW	V-shape	135	101	0.01101	-643	5
52	12.53799344	36.72525538	elliptical (E-W)	V-shape	149	100	0.01125	-645	4
53	12.54501960	36.72478098	elliptical (E-W)	V-shape	258	113	0.02095	-656	10

Table 2 - continued.

Id	Lon [d.ddd°E]	Lat [d.ddd°N]	Plan view	Cross-section	Major axis [m]	Minor axis [m]	Surface base [km²]	Top depth [m]	Depth [m]
54	12.55288683	36.72395171	elliptical (NE-SW)	V-shape	173	106	0.01688	-676	10
55	12.62071269	36.73119034	sub-circular	V-shape	101	100	0.00835	-672	8
56	12.72778325	36.69879844	sub-circular	V-shape	121	98	0.01015	-602	9
57	12.75305250	36.70560305	sub-circular	V-shape	221	189	0.03189	-587	15
58	12.75996046	36.69807909	sub-circular	V-shape	206	178	0.02933	-609	19
59	12.70153594	36.64035535	sub-circular	V-shape	160	132	0.01745	-729	10
60	12.70682374	36.63835505	sub-circular	V-shape	206	194	0.03247	-737	13
61	12.70982009	36.63578772	sub-circular	V-shape	108	102	0.00902	-741	6
62	12.75341534	36.61610240	elliptical (E-W)	V-shape	357	238	0.0655	-617	22
63	12.76615795	36.61116410	elliptical (E-W)	V-shape	109	68	0.00593	-593	6
64	13.10229381	36.67326520	sub-circular	V-shape	221	177	0.0314	-679	15
65	13.10731636	36.67190075	sub-circular	V-shape	174	194	0.02135	-677	11
66	13.11399164	36.67067719	sub-circular	V-shape	117	100	0.00924	-663	3
67	13.11663669	36.67018051	sub-circular	V-shape	144	134	0.01547	-660	7

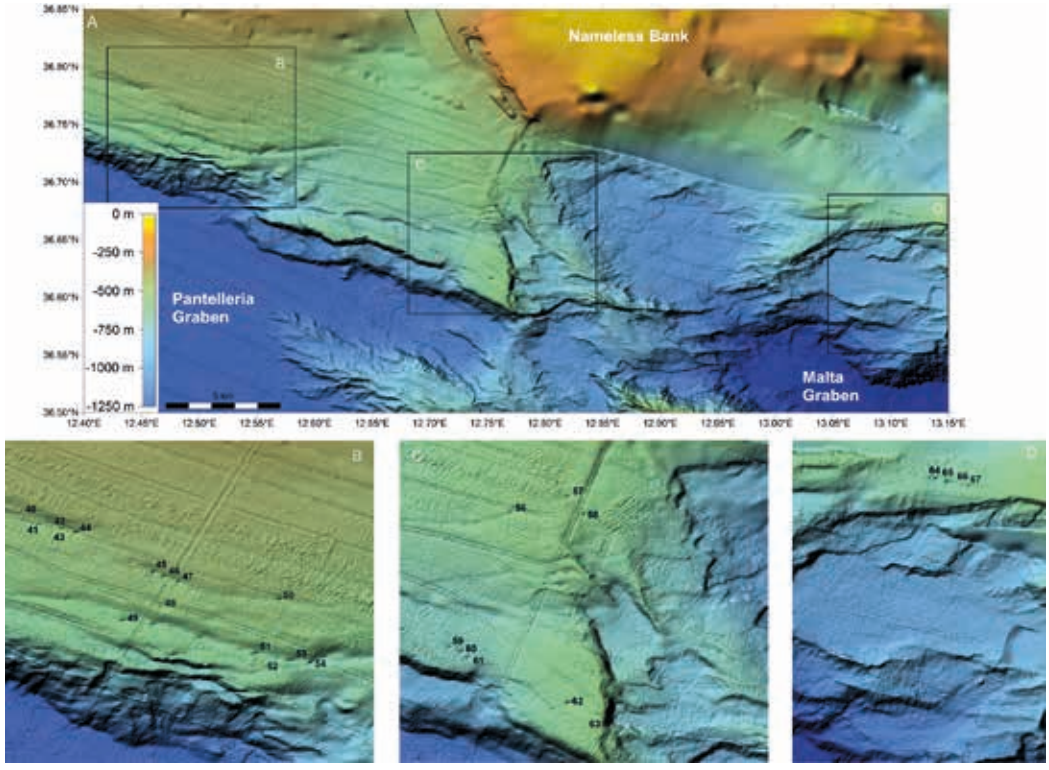

Fig. 10 - Negative features noted along the north-eastern edge of the Pantelleria Graben (A to C) and in the northernmost part of the north-eastern flank of the Malta Graben (A and D). Along the north-eastern side of the Pantelleria Graben, a total of 24 sub-circular depressions were identified (A to C, numbers 40-63). These depressions on the seabed, interpreted as pockmarks, generally form NW-SE alignments parallel to the graben axis controlled by normal faults with the same trend. The location of the main morpho-bathymetric map (A) is shown in Fig. 2.

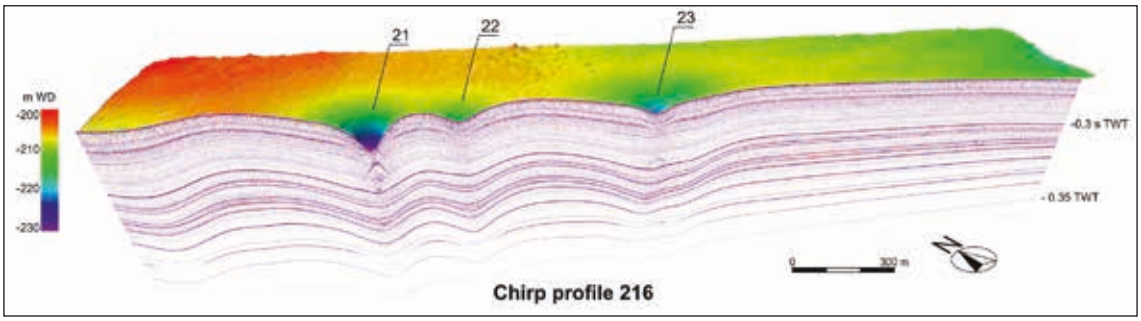

Fig. 11 - CHIRP profile 216, which crosses some negative features (numbers 21, 22 and 23), with the associated multibeam bathymetry. The subsurface character of the negative features consists of continuous high amplitude reflectors with a concave upward geometry. The presence of a hyperbolic anomalous distortion of the seismic reflectors indicates gas migration paths. The position of the seismic line is shown in Fig. 9C.

4.3 Erosional features

4.3.1. Submarine landslides

The available data show that there is a large landslide in the easternmost part of the Pantelleria Graben (Fig. 12). It is characterised by three contiguous landslide scars with associated mobilised

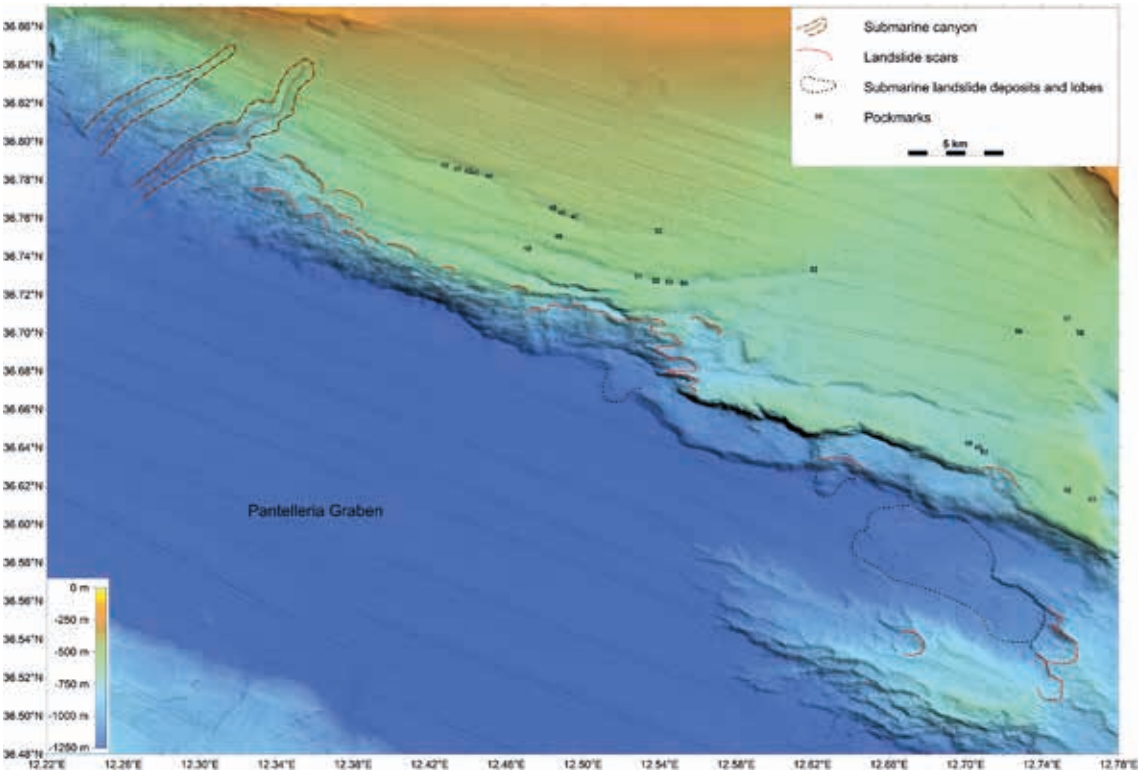

Fig. 12 - Erosional features (landslides and canyons) and pockmarks on the north-eastern flank of the Pantelleria Graben.

material. The scars cover an area of 4.3 km^2 in water depths ranging between 810 and 1150 m. The heads of the scars extend over 6.6 km. The scars have an overall smooth and concave surface with a variable slope between 8° and 15°, and their termination lies downslope with a distinct steepness of up to 60 m in height. The head-scarp has a maximum height of 250 m, while the maximum length of the scars, from the head of the landslide scar to the basal ramp, is up to 2.3 km. The scars are laterally bounded by linear, steep (up to 25°), up to 100 m high and WNW-trending escarpments, indicating a possible tectonic control on their development. The landslide deposits associated with these scars are located in water depths ranging between 1170 and 1280 m and cover an area of about 28 km^2. The distance between the landslide head and the landslide toe (30 m high) is about 11 km, while the maximum width is about 3.7 km. The morphology of the landslide deposits is rough, with the occurrence of small arcuate ridges in the distal part, indicating a N-W direction of movement. Other smaller scars with locally associated mobilised deposits can be seen along the NE margin of the Pantelleria Graben, all developed along the tectonic escarpment formed by the NW-trending normal faults that controlled the opening of this depression (Fig. 12).

4.3.2. Canyons

Two submarine canyons are visible along the slope connecting the AP with the Pantelleria Graben (Fig. 12). The largest extends for 11 km in the NE-SW direction and has a slightly sinuous course in the upper part and a maximum width of 2 km. It is located in water depths ranging between 470 and 1264 m, along a rim characterised by a slope of about 4°. The canyon does not affect the AP shelf and has an incised thalweg with a maximum depth of about 120 m and a maximum wall slope of 18°. The other canyon is located 3 km further NW and is less pronounced with a maximum width of 700 m and a total length of about 4 km. The head of the canyon lies in a water depth of 450-470 m, closest to the edge of the Pantelleria Graben.

5. Discussion and conclusions

The analysis of the dataset consisting of high-resolution multibeam echo-sounder and seismic data (CHIRP) collected in the western part of the SC has allowed to map and analyse various morphological features, highlighting the inherent complexity of this sector of the central Mediterranean. The occurrence and mutual influence of different geological processes, both shallow and intermediate, have been highlighted.

The Capo Granitola-Sciacca offshore area is a continental shelf hosting depositional bedforms characterised by opaque (Type 1 and 3) and semi-transparent (Type 2) seismic facies, probably composed of coarse-grained sediments such as sands. Furthermore, the opaque bodies do not have internal reflectors and their very low signal penetration probably indicates cemented sediments. In particular, the large elongated bodies of Type 1 (Figs. 3 and 4), visible only west of the Actea Volcano, can be interpreted as sand ridges occurring in a localised group, while the modest asymmetric bodies of Type 2 could be active and inactive sand dunes associated with the post-LGM transgressive phase (Figs. 3 and 5). These bodies are characterised by SW-ward prograding foresets. The arcuate and isolated sand deposits of Type 3 could be remnants of cords of dunes or of barrier lagoon systems eroded by the action of bottom currents (Figs. 3 and 6). The above bodies probably formed during the post-LGM sea-level rise, between ca. 18 kyr B.P. and 6 kyr B.P. (transgressive deposits), and during the glacial phase (lowstand deposits)

around 20 kyr B.P., when sea level was ca. 120-130 m lower than today (e.g. Siddal *et al*., 2003; Clarke *et al*., 2009). The positive feature of Type 4 consists of a low and rounded mound that, based on seismic facies and morphological characteristics, could represent a sedimentary wave composed of an alternation of coarse- and fine-grained sediments that typically deposit in areas where bottom currents flow through and where the seabed gradient changes (Figs. 3 and 7). Type 5 includes several mounds not associated with magnetic anomalies identified around the Actea and Nesea volcanoes (Fig. 8). These mounds, some of which are buried under a thin layer of recent sediments, lie on a folded pre-LGM succession and are associated with both subsurface gas features [gas seepage, blanking area, bright spots (Ferrante *et al*., 2022)] and local gas emissions in the water column. The CHIRP profiles show that these reliefs are active and deform the recent sedimentary layer. Moreover, in the area of Nesea Volcano, they form a 2-km-long N-S-oriented line developed over the faults associated with the SFS. These mounds have been interpreted as possible mud volcanoes generated by the rising of overpressure fluids and mud material along the faults and fractures associated with the active CGFS and SFS (Ferrante *et al*., 2022). Active mud volcanoes have also been identified in the eastern part of the Gela Basin, related to the tectonic structures of the Scicli fault zone (Holland *et al*., 2003), while active mud diapirs have been identified off the Sciacca and Agrigento coasts (Mancuso and Catalano, 2020).

To the west of the Nerita Bank, along the north-eastern side of the Pantelleria Graben, and in the area between the Graham and Terrible banks to the south, and the Doride Volcano to the north, numerous sub-circular/elliptical seabed depressions with a V-shaped transverse profile have been identified (Figs. 9 and 10). Their seismic characteristics (concave reflectors upwards), as well as evidence of migration and the presence of gas (Fig. 11), allowed these features to be interpreted as pockmarks formed by the release of over-pressurised fluids from the subsurface (e.g. Hovland *et al*., 2010). No evidence of fluid seepage in the water column would indicate a lack of recent activity in these structures, even if they are not overlain by recent sedimentation. As suggested by Ferrante *et al*. (2022), this could be due either to some kind of quiescence in fluid migration or to the effect of bottom currents preventing sediment deposition in seabed depressions. Evidence of pockmarks has already been reported in the studied area by other authors, particularly at Graham and Terrible banks (Spatola *et al*., 2018a, 2018b; Coltelli *et al*., 2016). The NW-oriented alignments of pockmarks identified along the northern flank of the Pantelleria Graben are probably controlled by normal faults with the same orientation associated with the opening of the graben itself (Fig. 10).

The numerous hydrocarbon fields of the SC (Granath and Casero, 2004) and the studies on the potential reservoirs (Civile *et al*., 2013) suggest a deep origin of the gas present in the study area, especially from the Meso-Cenozoic carbonate succession. Possible mixing with fluids of magmatic origin cannot be excluded, as also reported in Coltelli *et al*. (2016) for the emissions analysed at Graham Bank.

Erosional features consisting of scars have been identified along the northern margin of the Pantelleria Graben, characterised by the presence of high-angle fault-scarps (Fig. 12). A significant landslide, about 11 km long and 3.7 km wide, was identified in the easternmost part of the Pantelleria Graben. It was formed by three coalescent scars with the associated mobilised material that covers an area of about 28 km^2. Two submarine canyons cut the slope between the AP and the Pantelleria Graben, which has a gradient of about 4°. The largest of them extends for 11 km with a slightly sinuous course and a maximum depth of about 120 m; the other is less extensive and wider, testifying a weaker erosional activity.

The mud volcanoes identified in the Capo Granitola-Sciacca offshore, as well as the volcanoes and the numerous pockmarks visible throughout the study area, show a distribution that

clearly indicates tectonic control operated by the faults associated with the NNE-oriented active lithospheric structure, the CGSFZ, and the normal faults responsible for the opening of the Pantelleria Graben. Moreover, the presence of these elements, together with the identification of bright spots, areas of signal blanking and local gas emissions on the seafloor in the CHIRP profiles, may indicate the presence of a significant gas accumulation in the upper part of the stratigraphic sequence.

Considering the literature information and the origin of the hydrocarbon fields exploited in the SC, the explanation for the presence of gas is mainly assumed to be a thermogenic deep origin, especially from the Meso-Cenozoic carbonate succession, although mixing with fluids of magmatic origin cannot be excluded.

The morphological elements that we have mapped and described in this work, based on all the available high-resolution geophysical information, testify, although not yet completely, to the remarkably complex recent geological processes in the area. Some of these morphologies, such as volcanoes, mud volcanoes and fluid seeps, are located a short distance from the SW coasts of Sicily and therefore represent potential geological hazards that should be assessed through a comprehensive monitoring campaign and geophysical mapping.

Acknowledgments. This work benefited from the suggestions and comments of two reviewers. We also thank the editor D. Slejko for the support received.

REFERENCES

Antonelli M., Franciosi R., Pezzi G., Querci A., Ronco G.P. and Vezzani F.; 1988: *Paleogeographic evolution and structural setting of the northern side of the Sicily Channel.* Mem. Soc. Geol. It., 41, 141-157.

Argnani A.; 1990: *The Strait of Sicily rift zone: foreland deformation related to the evolution of a back-arc basin.* J. Geodyn., 12, 311-331.

Argnani A.; 2009: *Evolution of the southern Tyrrhenian slab tear and active tectonics along the western edge of the Tyrrhenian subducted slab*. In: Van Hinsbergen D.J.J., Edwards M.A. and Govers R. (eds), Collision and Collapse at the Africa-Arabia-Eurasia Subduction Zone, Geological Society London, London, UK, Special Publications 311, pp. 193-212, doi: 10.1144/SP311.7.

Argnani A., Cornini S., Torelli L. and Zitellini N.; 1986: *Neogene-Quaternary foredeep system in the Strait of Sicily*. Mem. Soc. Geol. It., 36, 123-130.

Ben-Avraham Z., Woodside J., Lodolo E., Gardosh M., Grasso M., Camerlenghi A. and Vai G.B.; 2006: *Eastern Mediterranean basin systems.* In: Gee D.G. and Stephenson R.A. (eds), European Lithosphere Dynamics, Geological Society London Memoirs, London, UK, vol. 32, pp. 263-276, doi: 10.1144/GSL.MEM.2006.032.01.39.

Boccaletti M., Cello G. and Tortorici L.; 1987: *Transtensional tectonics in the Sicily Channel.* J. Struct. Geol., 9, 869-876.

Borsetti A.M., Colantoni P. and Zarudzki F.K.; 1974: *Note strutturali e stratigrafiche sul Canale di Sicilia*. Mem. Soc. Geol. It., 13, 221-232.

Bosman A., Calarco M., Casalbore D., Chiocci F.L., Coltelli M., Conte A.M., Martorelli E., Romagnoli C. and Sposato A.; 2008: *Submarine volcanic features in the Pantelleria offshore revealed by high-resolution swath bathymetry.* Rend. Soc. Geol. It., 3, 128-129.

Burollet P.F., Mugniot J.M. and Sweeney P.; 1978: *The geology of the Pelagian block: the margins and basins of southern Tunisia and Tripolitania*. In: Nairn A.E.M., Kanes W.H. and Stelhi F.G. (eds), The Ocean Basins and Margins: The Western Mediterranean., Vol. 4b. Plenum, New York, NY, USA, pp. 331-359.

Calanchi N., Colantoni P., Rossi P.L., Saitta M. and Serri G.; 1989: *The Strait of Sicily continental rift systems: physiography and petrochemistry of the submarine volcanic centres*. Mar. Geol., 87, 55-83.

Calò M. and Parisi L.; 2014: *Evidence of a lithospheric fault zone in the Sicily Channel continental rift (southern Italy) from instrumental seismicity data*. Geophys. J. Int., 199, 219-225.

Catalano R., Di Stefano P., Sulli A. and Vitale F.P.; 1996: *Paleogeography and structure of the central Mediterranean: Sicily and its offshore area*. Tectonophys., 260, 291-323.

Catalano R., Merlini S. and Sulli A.; 2002: *The structure of western Sicily, central Mediterranean*. Pet. Geosci., 8, 7-18.

Catalano R., Valenti V., Albanese C., Accaino F., Sulli A., Tinivella U., Morticelli M.G., Zanolla C. and Giustiniani M.; 2013: *Sicily's fold-thrust belt and slab roll.back: the SI.RI.PRO. seismic crustal transect*. J. Geol. Soc. London, 170, 451-464.

Cavallaro D. and Coltelli M.; 2019: *The Graham volcanic field offshore Sicily (Italy) revealed by high-resolution seafloor mapping and ROV images.* Front. Earth Sci., 7, 311, doi: 10.3389/feart.2019.00311.

Cavallaro D., Monaco C., Polonia A., Sulli A. and Di Stefano A.; 2017: *Evidence of positive tectonic inversion in the north-central sector of the Sicily Channel (central Mediterranean).* Nat. Hazards, 86, S233-S251, doi: 10.1017/s11069-016-2515-6.

Civile D., Lodolo E., Accettella D., Geletti R., Ben-Avraham Z., Deponte M., Facchin L., Ramella R. and Romeo R.; 2010: *The Pantelleria graben (Sicily Channel, central Mediterranean): an example of intraplate "passive" rift.* Tectonophys., 490, 173-183, doi: 10.1016/j.tecto.2010.05.008.

Civile D., Zecchin M., Forlin E., Donda F., Volpi V., Merson B. and Persoglia S.; 2013: *CO2 geological storage in the Italian carbonate successions.* Int. J. Greenhouse Gas Control, 19, 101-116, doi: 10.1016/j.ijggc.2013.08.010.

Civile D., Lodolo E., Alp H., Ben-Avraham Z., Cova A., Baradello L., Accettella D., Burca M. and Centonze J.; 2014: *Seismic stratigraphy and structural setting of the Adventure Plateau (Sicily Channel).* Mar. Geophys. Res., 35, 37-53, doi: 10.1007/s11001-013-9205-5.

Civile D., Lodolo E., Zecchin M., Ben-Avraham Z., Baradello L., Accettella D., Cova A. and Caffau M.; 2015: *The lost Adventure Archipelago (Sicilian Channel, Mediterranean Sea): morpho-bathymetry and Late Quaternary palaeogeographic evolution.* Global Planet. Change, 125, 36-47, doi: 10.1016/j.gloplacha.2014.12.003.

Civile D., Lodolo E., Caffau M., Baradello L. and Ben-Avraham Z.; 2016: *Anatomy of a submerged archipelago in the Sicilian Channel (central Mediterranean Sea)*. Geol. Mag., 153, 160-178, doi: 10.1017/S0016756815000485.

Civile D., Lodolo E., Accaino F., Geletti R., Schiattarella M., Giustiniani M., Fedorik J., Zecchin M. and Zampa L.; 2018: *Capo Granitola-Sciacca Fault Zone (Sicilian Channel, central Mediterranean): structure vs magmatism.* Mar. Pet. Geol., 96, 627-644, doi: 10.1016/j.marpetgeo.2018.05.016.

Civile D., Brancolini G., Lodolo E., Forlin E., Accaino F., Zecchin M. and Brancatelli G.; 2021: *Morphostructural setting and tectonic evolution of the central part of the Sicilian Channel (central Mediterranean).* Lithos, 2021, 7866771, 24 pp., doi: 10.2113/2021/7866771.

Clarke P.U., Dyke A.S., Shakum J.D., Carlson A.E., Clark J., Wohlfarth B., Mitrovica J.X., Hostetler S.W. and McCabe A.M.; 2009: *The last glacial maximum*. Sci., 325, 710-714.

Colantoni P.; 1975: *Note di geologia marina sul Canale di Sicilia.* Giornale di Geologia, 40, 181-207.

Colantoni P., Del Monte M., Gallignani P. and Zarudzky E.F.K.; 1975: *Il Banco Graham: un vulcano recente nel Canale di Sicilia.* Giornale di Geologia, 40, 141-162.

Colantoni P., Cremona G., Ligi M., Borsetti A.M. and Cati F.; 1985: *The Adventure Bank (off south-western Sicily): a present-day example of carbonate shelf sedimentation*. Giornale di Geologia, 47, 165-180.

Coltelli M., Cavallaro D., D'Anna G., D'Alessandro A., Grassa F., Mangano G., Patanè D. and Gresta S.; 2016: *Exploring the submarine Graham Bank in the Sicily Channel*. Ann. Geophys., 59, S0208, doi: 10.4401/ag-6929.

Corti G., Cuffaro M., Doglioni C., Innocenti F. and Manetti P.; 2006: *Coexisting geodynamic processes in the Sicily Channel.* Geol. Soc. Am., Special paper 409, 83-96.

Falzone G., Lanzafame G. and Rossi P.L.; 2009: *Il vulcano Ferdinandea nel Canale di Sicilia*. Geoitalia, 29, 15-20.

Fedorik J., Toscani G., Lodolo E., Civile D., Bonini L. and Seno S.; 2018: *Structural analysis and Miocene-to-present tectonic evolution of a lithospheric-scale, transcurrent lineament: the Sciacca Fault (Sicilian Channel, central Mediterranean Sea).* Tectonophys., 722, 342-355, doi: 10.1016/j.tecto.2017.11.014.

Ferrante G.M., Accaino F., Civile D., Lodolo E., Volpi V., Romeo R. and Accettella D.; 2022: *Deep and shallow gas occurrence in the NW Sicilian Channel and related features.* Mar. Pet. Geol., 139, 1-13, doi: 10.1016/j.marpetgeo.2022.105575.

Ferranti L., Pepe F., Barreca G., Meccariello M. and Monaco C.; 2019: *Multi-temporal tectonic evolution of Capo Granitola and Sciacca foreland transcurrent faults (Sicily Channel).* Tectonophys., 765, 187-204, doi: 10.1016/j.tecto.2019.05.002.

Finetti I.R. and Del Ben A.; 2005: *Crustal tectono-stratigraphic setting of the Pelagian foreland from new CROP seismic data*. In: Finetti I.R. (ed), CROP Project: Deep Seismic Exploration of the Central Mediterranean and Italy, Elsevier, Amsterdam, The Netherlands, pp. 581-595.

Ghisetti F.C., Gorman A.R., Grasso M. and Vezzani L.; 2009: *Imprint of foreland structure on the deformation of a thrust sheet: the Plio-Pleistocene Gela Nappe (southern Sicily, Italy).* Tectonics, 28, TC4015, doi: 10.1029/2008TC002385.

Granath J.W. and Casero P.; 2004: *Tectonic setting of the petroleum systems of Sicily.* In: Swennen R., Roure F. and Granath J.W. (eds), Deformation, fluid flow, and reservoir appraisal in foreland fold and thrust belts, AAPG Hedberg Series, 1, pp. 391-411, doi: 10.1306/1025702H1854.

Holland C., Etiope G., Milkov A. and Michelozzi E.; 2003: *Mud volcanoes discovered offshore Sicily.* Mar. Geol., 199, 1-6, doi: 10.1016/S0025-3227(03)00125-7.

Hovland M., Heggland R., De Vries M.H. and Tjelta T.I.; 2010: *Unit-pockmarks and their potential significance for predicting fluid flow.* Mar. Pet. Geol., 27, 1190-1199, doi: 10.1016/j.marpetgeo.2010.02.005.

Jongsma D., Van Hinte J.E. and Woodside J.M.; 1985: *Geologic structure and neotectonics of the North African continental margin south of Sicily.* Mar. Pet. Geol., 2, 156-179, doi: 10.1016/0264-8172(85)90005-4.

Lodolo E., Civile D., Zanolla C. and Geletti R.; 2012: *Magnetic signature of the Sicily Channel volcanism.* Mar. Geophys. Res., 33, 33-44, doi: 10.1007/s11001-011-9144-y.

Lodolo E., Sanfilippo R., Rajola G., Canese S., Andaloro F., Montagna P., Rosso A., Macaluso D., Di Geronimo I. and Caffau M.; 2017: *The red coral deposits of the Graham Bank area: constraints on the Holocene volcanic activity of the Sicilian Channel.* GeoResJ, 13, 126-133, doi: 10.1016/j.grj.2017.04.003.

Lodolo E., Civile D., Zecchin M., Zampa L.S. and Accaino F.; 2019a: *A series of volcanic edifices discovered a few kilometers off the coast of SW Sicily*. Mar. Geol., 416, 105999, doi: 10.1016/j.margeo.2019.105999.

Lodolo E., Zampa L. and Civile D.; 2019b: *The Graham and Terrible volcanic province (NW Sicilian Channel): gravimetric constraints for the magmatic manifestations.* Bull. Volcanol., 81, 1-11, doi: 10.1007/s00445-019-1274-0.

Lodolo E., Galassi G., Spada G., Zecchin M., Civile D. and Bressoux M.; 2020: *Post-LGM coastline evolution of the NW Sicilian Channel: comparing high-resolution geophysical data with Glacial Isostatic Adjustment modeling.* PLoS ONE, 15, e0228087, doi: 10.1371/journal.pone.0228087.

Lodolo E., Renzulli A., Cerrano C., Calcinai B., Civile D., Quarta G. and Calcagnile L.; 2021: *Unraveling past submarine eruptions by dating lapilli tuff-encrusting coralligenous (Actea volcano, NW Sicilian Channel).* Front. Earth Sci., 9, 664591, doi: 10.3389/feart.2021.664591.

Lodolo E., Loreto M.F., Melini D., Spada G. and Civile D.; 2022: *Palaeo-Shoreline configuration of the Adventure Plateau (Sicilian Channel) at the Last Glacial Maximum.* Geosci., 12, 125, doi: 10.3390/geosciences12030125.

Mancuso M.R. and Catalano R.; 2020: *Evidenze sismostratigrafiche di fenomeni da espulsione di fluidi, superficiali e profondi, nell'offshore tra Sciacca e Agrigento (Sicilia meridionale).* Mem. Descr. Carta Geol. d'It., 105, 97-102.

Palano M., Ursino A., Spampinato S., Sparacino F., Polonia A. and Gasperini L.; 2020: *Crustal deformation, active tectonics and seismic potential in the Sicily Channel (central Mediterranean), along the Nubia-Eurasia plate boundary.* Sci. Rep., 10, 21238, doi: 10.1038/s41598-020-78063-1.

Reuther C.D., Ben-Avraham Z. and Grasso M.; 1993: *Origin and role of major strike-slip transfers during plate collision in the central Mediterranean.* Terra Nova, 5, 249-257, doi: 10.1111/j.1365-3121.1993.tb00256.x.

Romagnoli C., Belvisi V., Innangi S., Di Martino G. and Tonielli R.; 2020: *New insights on the evolution of the Linosa Volcano (Sicily Channel) from the study of its submarine portions.* Mar. Geol., 419, 106060, doi: 10.1016/j.margeo.2019.106060.

Siddall M., Rohling E.J., Almogi-Labin A., Hemleben C., Meischner D., Schmelzer I. and Smeed D.A.; 2003: *Sea-level fluctuations during the last glacial cycle.* Nature, 423, 853-858, doi: 10.1038/nature01690.

Spatola D., Micallef A., Sulli A., Basilone L. and Basilone G.; 2018a: *Evidence of active fluid seepage (AFS) in the southern region of the central Mediterranean Sea*. Meas., 128, 247-253, doi: 10.1016/j.measuyrement.2018.06.058.

Spatola D., Micallef A., Sulli A., Basilone L., Ferreri R., Basilone G., Bonanno A., Pulizzi M. and Mangano S.; 2018b: *The Graham Bank (Sicily Channel, central Mediterranean Sea): seafloor signatures of volcanic and tectonic controls.* Geomorphol., 318, 375-389, doi: 10.1016/j.geomorph.2018.07.006.

Corresponding author: Valentina Volpi
Istituto Nazionale di Oceanografia e di Geofisica Sperimentale - OGS
Borgo Grotta Gigante 42C, 34010 Sgonico (TS), Italy
Phone: +39 040 2140361; e-mail: vvolpi@ogs.it